

Spectrum and energy levels of the high-lying singly excited configurations of Nd III[★]

New Nd III experimental energy levels and wavelengths, and transition probability and ionisation energy calculations

M. Ding¹, A. N. Ryabtsev², E. Y. Kononov², T. Ryabchikova³, and J. C. Pickering¹

¹ Physics Department, Imperial College London, Prince Consort Road, London, SW7 2AZ, UK
e-mail: milan.ding15@imperial.ac.uk

² Institute of Spectroscopy, Russian Academy of Sciences, Troitsk, Moscow, 108840, Russia

³ Institute of Astronomy, Russian Academy of Sciences, Pyatnitskaya 48, Moscow 119017, Russia

Received ?; accepted ?

ABSTRACT

Aims. To accurately determine bound-to-bound transition wavelengths and energy levels of the high-lying open-shell configurations $4f^37s$, $4f^36d$, and $4f^35f$ of doubly-ionised neodymium (Nd III, $Z = 60$) through high-resolution spectroscopy and semi-empirical calculations.

Methods. Fourier transform spectra of Nd Penning and hollow cathode discharge lamps were recorded within the region $32\,500\text{--}54\,000\text{ cm}^{-1}$ ($3077\text{--}1852\text{ \AA}$) and grating spectra of Nd vacuum sliding sparks were recorded within the regions $820\text{--}1159\text{ \AA}$ and $1600\text{--}3250\text{ \AA}$. New energy levels were found using the observed wavelengths measured accurate to a few parts in 10^8 in Fourier transform spectra and to a few parts in 10^7 in grating spectra. Atomic structure and transition probability calculations of Nd III were made using the Cowan codes by adjusting energy parameters to fit all known Nd III levels. Nd-rich stellar spectra were also used to evaluate the new calculations.

Results. In total, 355 transitions were classified from observed spectra involving 116 previously experimentally unknown energy levels of the $4f^37s$, $4f^36d$, and $4f^35f$ configurations of Nd III, all reported here for the first time. One newly identified level of the $4f^35d$ configuration is also reported. Typical level energy uncertainties are 0.01 cm^{-1} for the $4f^37s$ and $4f^36d$ levels and 0.3 cm^{-1} for the $4f^35f$ levels. In addition, calculated energy levels up to $130\,936\text{ cm}^{-1}$ are presented, including eigenvector composition and calculated level lifetimes. Calculated transition probabilities and wavelengths between $1900\text{--}50\,000\text{ \AA}$ are also presented. Using newly established levels of the $4f^37s$ configuration and the recently established levels of the $4f^36s$ configuration, the ionisation energy of Nd III was estimated at $178\,090 \pm 330\text{ cm}^{-1}$, doubling the accuracy of the previously published value.

Conclusions. These results will enable more accurate analyses of astrophysical plasmas involving the Nd III ion, such as in chemically peculiar stars and kilonovae. Results from the Cowan code calculations will also aid the identification of Nd III transitions unobserved in the laboratory spectra of this work and support transition probability measurements of Nd III.

Key words. Atomic data – Line: identification – Methods: laboratory: atomic – Methods: data analysis – Stars: abundances – Stars: chemically peculiar

1. Introduction

Accurate and complete knowledge of atomic spectra of the lanthanide elements ($Z = 57 - 71$) is necessary for a variety of astronomical applications. For example, in reliable astrophysical chemical abundance analyses in spectroscopic studies of chemically peculiar stars (e.g., Przybylski 1977; Cowley et al. 2000; Ryabchikova et al. 2006) and their pulsational wave propagations (e.g., Savanov et al. 1999). Wavelengths of the spectral lines used in these analyses must be known with accuracies matching or exceeding those provided by the existing and planned high-resolution modern ground and space-based telescopes with resolving powers of up to 10^5 . Importantly, in disentangling the spectra of kilonovae (e.g., Kasen et al. 2013; Tanaka & Hotokezaka 2013; Smartt et al. 2017; Tanaka et al. 2018; Watson et al. 2019; Gaigalas et al. 2019; Tanaka et al. 2020; Even

et al. 2020; Cowan et al. 2021; Domoto et al. 2022), the spectral data of the lanthanide elements of the first few ionisation stages also need to be as complete and as accurate as possible.

Experimental investigation of the atomic structure of the lanthanide elements using high-resolution spectroscopy is a key step in addressing the need for complete and accurate knowledge of their spectral data. Not only do the measured transition wavelengths fulfill the accuracy requirements, but the experimentally established energy levels also allow accurate transition probability (TP) measurements or calculations to be undertaken, e.g., in the present work, semi-empirical calculations were made from adjusting energy parameters of the Cowan codes (Cowan 1981; Kramida 2021) to optimise prediction of the level energies and eigenvector compositions that are used for calculations of theoretical TPs.

The original experimental investigations of Nd III atomic structure were by Dieke et al. (1961) and Dieke & Cross-

* All tables are available in full at the CDS.

white (1963), which were later extended by Aldenius (2001), Ryabchikova et al. (2006), and Ding et al. (2024). This paper reports the continuation and extension of the work of Ding et al. (2024) that had reported the classification of 623 transitions of 105 new and 39 improved energy levels of the $4f^4$, $4f^35d$, $4f^36s$, and $4f^36p$ configurations of Nd III. In the present work, 355 additional transitions of Nd III are further classified by Fourier transform (FT) and grating spectroscopy of Nd discharge sources, which determine 116 new energy levels of the $4f^37s$, $4f^36d$, and $4f^35f$ configurations for the first time. The further analysis of stellar absorption spectra of Nd III has also led to the identification of one new $4f^35d$ level, increasing the total number of known levels of Nd III now to 261.

All level energies of the $4f^37s$ and $4f^36d$ configurations are determined by transition wavenumbers measured by FT spectroscopy of a Nd Penning discharge lamp (PDL) (e.g., Finley et al. 1979; Heise et al. 1994) within the region $32\,500\text{--}54\,000\text{ cm}^{-1}$ ($3077\text{--}1852\text{ \AA}$), accurate to a few parts in 10^8 . All level energies of the $4f^35f$ configuration are determined by grating spectroscopy of Nd vacuum sliding spark (VS) discharges within the region $820\text{--}1159\text{ \AA}$, accurate to a few parts in 10^7 .

The ionisation energy is one of the fundamental constants of an ion, which is also important for modelling astrophysical plasma conditions. Adopting the method from Sugar & Reader (1973), the Nd III ionisation energy is estimated to be $178\,070 \pm 330\text{ cm}^{-1}$ using previously unknown experimental level energies.

2. Experimental details

Full experimental details of the majority of the atomic emission spectra analysed in the present work are in Ding (2024) and Ding et al. (2024), therefore only a summary is provided here. Prior to wavelength and relative intensity calibration, the wavelengths and relative intensities of each spectral line were obtained by fitting the spectra using model line profiles, and resulting line parameters were tabulated as line lists for the subsequent energy level analysis.

2.1. Fourier transform spectroscopy of Nd

The FT spectra used in this work were the two Nd-Ar PDL spectra measured in and labelled as E and F in Table 2 of Ding et al. (2024), covering the regions $32\,480\text{--}44\,422\text{ cm}^{-1}$ ($3079\text{--}2251\text{ \AA}$) and $44\,422\text{--}53\,822\text{ cm}^{-1}$ ($2251\text{--}1858\text{ \AA}$), respectively. These were recorded on the high-resolution $f/25$ Imperial College VUV FT spectrometer (Thorne et al. 1987), at resolutions 0.07 and 0.08 cm^{-1} respectively, which were chosen such that the resolving power was limited by the Doppler width of the PDL spectral lines. The PDL cathodes were 99.5% pure Nd and run with argon carrier gas at a current of 750 mA for both spectra and at pressures of 1.7×10^{-3} and $2.0 \times 10^{-3}\text{ mbar}$ respectively. The observed wavenumbers were calibrated using Ar II standard lines recommended by Learner & Thorne (1988) and measured by Whaling et al. (1995). The wavenumber uncertainties of non-blended, non-self-absorbed lines with signal-to-noise ratio (S/N) greater than 100 were no more than 0.003 cm^{-1} ($\sim 0.0003\text{ \AA}$ at 3000 \AA). The spectra were intensity calibrated to a relative scale using a deuterium standard lamp. Two Nd-Ar hollow cathode lamp (HCL) spectra had also been recorded in exactly the same spectral regions in Ding et al. (2024). The $4f^36p - 4f^37s$ and $4f^36p - 4f^36d$ transitions used in the present work to find the $4f^37s$ and $4f^36d$ levels were notably not observed in these two

HCL spectra, and this aided their classifications as one would expect transitions from higher-lying levels to be lower in intensity in the hollow cathode lamp due to its lower effective temperature and hence correspondingly lower level populations for higher-lying levels compared to the PDL.

2.2. Grating spectroscopy of Nd

The grating spectra used in this work include all four Nd VS spectra presented in Table 4 of Ding et al. (2024), and these were recorded at VS currents up to 1500 A . Two of these spectra were recorded using the 6.65 m normal incidence spectrograph at the Institute of Spectroscopy in Troitsk using photographic plates, spanning the regions $390\text{--}1525\text{ \AA}$ and $1600\text{--}2536\text{ \AA}$. The other two spectra were recorded using the 10 m normal incidence spectrograph at the National Institute of Standards and Technology (NIST), covering $2330\text{--}3250\text{ \AA}$, also using photographic plates. Impurity lines of oxygen, carbon, nitrogen, and silicon in various ionisation stages (Kramida et al. 2022), as well as lines of Nd IV (Wyart et al. 2007) and Nd V (Meftah et al. 2008), were used for wavelength calibration in the range $390\text{--}1525\text{ \AA}$. The other grating spectra were wavelength calibrated using Nd III Ritz wavelengths determined in Ding et al. (2024). Relative intensities were calibrated using approximate plate response curves and sensitivities. The wavelength uncertainty was estimated at $\pm 0.006\text{ \AA}$ using the RMS deviations of wavelengths from corresponding reference wavelengths. Due to the much higher currents of the VS discharges, the weaker transitions from high-lying Nd III levels that were either around the noise level or absent in the Nd-Ar PDL FT spectra were of moderate intensity in the Nd VS grating spectra.

Additionally, a line list of a grating spectrum in the range $820\text{--}1159\text{ \AA}$ was used (Wyart 2006). This spectrum was recorded using a VS in the sliding mode of operation at 200 A current on the NIST 10-m normal incidence spectrograph. The wavelength uncertainty of this spectrum was estimated at $\pm 0.006\text{ \AA}$ using the RMS of differences between wavelengths of Nd III lines in this spectrum and the spectrum from Troitsk in the range $390\text{--}1525\text{ \AA}$. The Troitsk Nd VS spectrum was taken at 1500 A and has a much higher background, many weaker lines were not observed and some lines were also blended with the second-order lines with shorter wavelengths. Therefore, the additional line list of Wyart (2006) in the range $820\text{--}1159\text{ \AA}$ was used for wavelength measurements of the $4f^35d - 4f^35f$ transitions.

3. Empirical spectrum analysis of Nd III

3.1. Methodology

The empirical spectrum analysis of an atom or ion involves assigning upper and lower energy levels, i.e., a pair of energies and a pair of J values, to each of its transitions observed in the laboratory. This can be done by matching observed wavelengths of spectral lines with theoretical level energy separations, and by matching observed relative intensities of spectral lines with theoretical TPs and expected relative level populations. Such an analysis requires information on the spectrum of atomic transitions to be extracted into line lists by fitting experimental spectra using model line profiles. A line list contains the important parameters for each line, namely the wavenumber and relative intensity and their uncertainties. Other parameters such as S/N and FWHM are also a part of the line lists as these can hint at

potential problems with the fitted lines, such as unreliable weak and blended lines.

The matching of intensity patterns and level energy values to find new energy levels can be ambiguous in complex atomic spectra where the number of spurious candidate energy levels increases rapidly with increasing number of lines and increasing experimental and theoretical uncertainties in energies and relative intensities. Extra observational evidence is often required for correct line classifications. The methodology and strategies employed for the analysis of Nd III are discussed in detail in [Ding et al. \(2024\)](#).

3.2. Results

3.2.1. Energy levels

All newly found level energies of the $4f^37s$ and $4f^36d$ configurations were optimised by inputting wavenumbers of 579 Nd III lines fitted from the Nd-Ar PDL FT spectra ([Ding et al. 2024](#)) into the computer program LOPT by [Kramida \(2011\)](#), where level energy uncertainties, Ritz wavenumbers, and Ritz wavenumber uncertainties were also estimated. All newly found $4f^35f$ level energies were estimated using transition wavelengths recorded by [Wyart \(2006\)](#) in the range 820–1159 Å and input into LOPT with the connecting $4f^35d$ levels at fixed energies. The differences between fixing and not fixing the $4f^35d$ level energies are negligible due to the much higher uncertainties of the $4f^35d - 4f^35f$ grating wavelengths. This fixing of $4f^35d$ levels was chosen as the higher-resolution FT measurements used to find the $4f^35d$ levels in [Ding et al. \(2024\)](#) are more reliable, i.e., higher accuracy and better-resolved blends.

The 116 newly identified energy levels of the $4f^37s$, $4f^36d$, and $4f^35f$ configurations of Nd III are included in Table 1. The extract of Table 1 shows the lowest-lying levels of these configurations and energy ranges of the table for both parities. Typical energy uncertainties are 0.01 cm^{-1} for the $4f^37s$ and $4f^36d$ levels and 0.3 cm^{-1} for the $5f$ levels. We would like to note that the $4f^3(4I^\circ)6d \ ^5H_3$ level has relatively large energy uncertainty because the two lines observed for this level were blended with other lines in both the Nd-Ar PDL FT and the Nd VS grating spectra. The FWHM of each of the two lines in the FT spectrum was set as their statistical wavenumber uncertainties in the level energy optimisation.

In theoretical calculations, the $4f^37s$ levels were represented very well by the eigenfunctions from jj -coupling the excited electron with the three $4f$ core electrons in the LS -coupling scheme, similar to the $4f^36s$ levels of Nd III. The mean difference between all observed level energies and those from previous calculations in the literature by [Gaigalas et al. \(2019\)](#) was offset within a few percent (around 6000 cm^{-1}), but the variance in these differences within each configuration was up to two orders of magnitude smaller than the offset.

3.2.2. Classified transitions

In the Nd-Ar PDL FT spectra, 147 $4f^36p - 4f^37s$ and $4f^36p - 4f^36d$ Nd III transitions were observed, all of which were also observed in the Nd VS spectra and are listed in Table 2 with the maximum S/N at 37 and an average uncertainty of $\pm 0.024 \text{ cm}^{-1}$. The 39 lines of the $4f^36p - 4f^37s$ and $4f^36p - 4f^36d$ transition and 169 lines of the $4f^35d - 4f^35f$ transitions observed only in the Nd VS spectra are also listed in Table 2. The 39 grating lines originating from the $4f^37s$ and $4f^36d$ configurations were weighted zero in the level energy optimisation process; the

wavelength uncertainty of these grating spectra, deduced from RMS of deviations from reference wavelengths at $\pm 0.006 \text{ \AA}$, is around $\pm 0.1 \text{ cm}^{-1}$ at $40\,000 \text{ cm}^{-1}$, which is an order of magnitude higher than the $4f^37s$ and $4f^36d$ level energy uncertainties optimised purely using Nd-Ar FT spectra wavenumbers. Additionally, blends are much more common in the line-rich and lower-resolution Nd VS spectra, and therefore uncertainty improvements in the optimised level energies would not be guaranteed in the inclusion of these grating lines in the level optimisation process. For the $4f^35d - 4f^35f$ transitions observed only in the Nd VS grating spectra, their wavelength uncertainties of around $\pm 0.006 \text{ \AA}$ were used in level optimisation.

We would like to note that the relative intensity measurements in Table 2 are recommended only as guides ([Ding et al. 2024](#)). For the FT spectral lines, we estimate relative intensity uncertainties of at least 20% due to low S/Ns. These are also expected to be larger when comparing lines between FT spectra E and F, primarily due to the different lamp conditions on different days. For the grating spectral lines, the uncertainties are expected to be even more uncertain, and relative intensities are recommended to be qualitative as these are the photographic plate darkening calibrated using approximate sensitivity and grating instrumental response curves.

3.3. Analysis and remarks

We discuss the analysis and finding of the new energy levels of this work in this section. We expect most energy levels to be correctly identified and that they will improve current constraints and benchmarks for large-scale Nd III atomic structure calculations. For the $4f^36d$ levels with only one observed transition in Table 2, caution is advised and they should be more appropriately treated as tentative. For each of the $4f^36d$ levels of this category, the strongest transition to the $4f^36p$ configuration was observed across both the Nd-Ar PDL FT and Nd VS grating spectra and was the only candidate within $\sim 50 \text{ cm}^{-1}$ of the predicted wavenumber.

3.3.1. Finding $4f^3(2H^\circ)5d \ ^3F^\circ_4$ in stellar spectra

One additional level of the previously known $4f^35d$ configuration is newly identified based on the fitting of calculated line intensities and Zeeman patterns to the absorption line profiles in stellar spectra described in [Ding et al. \(2024\)](#). It is given the label $4f^3(2H^\circ)5d \ ^3F^\circ_4$ with energy estimated at $34\,742.15 \pm 0.10 \text{ cm}^{-1}$. Two transitions from $4f^3(2H^\circ)5d \ ^3F^\circ_4$ to known levels $4f^4 \ ^5F_5$ (4642.97 \AA , the stronger line) and $4f^4 \ ^3H_4$ (5517.27 \AA , the weaker line) were found in stellar spectra, their fits are shown in Fig. 1. The stronger transition is the only transition observed in the Nd-Ar FT spectra, but appeared blended in both the PDL and HCL spectra.

3.3.2. Initial Cowan code parameters

Before the experimental investigation of the $4f^37s$, $4f^36d$, and $4f^35f$ levels, theoretical atomic structure calculations for these configurations were made using the Cowan codes ([Cowan 1981](#); [Kramida 2021](#)), as these would guide the process of finding levels. The scaling factors of the $4f^36d$ configurations in these Cowan code calculations were taken as those fitted for the $4f^35d$ configuration. Parameters describing the interactions within the $4f^3$ sub-shell in the $4f^37s$ and $4f^35f$ configurations were also taken from their empirical ratios determined for the $5d$ config-

Table 1. Energy levels experimentally established and semi-empirically calculated for Nd III (extract).

Par.	Label	J	E_e (cm^{-1})	ΔE (cm^{-1})	τ (ns)	g^l	Eigenvector Composition (%)		
(1)	(2)	(3)	(4)	(5)	(6)	(7)	(8)		
e	$4f^4\ ^5I$	4	0.000(*)	4.2		0.604	97 $4f^4\ ^5I$		
⋮	⋮	⋮	⋮	⋮	⋮	⋮	⋮	⋮	⋮
e	$4f^3(^4I^\circ)5f\ ^5L$	6	114 016.4(6)	-4.8	5.2×10^{-10}	0.760	79 $4f^3(^4I^\circ)5f\ ^5L$	13 $4f^3(^4I^\circ)5f\ ^5K$	2 $4f^3(^2H2^\circ)5f\ ^3K$
e	$4f^3(^4I^\circ)5f\ ^5M$	7	114 015.1(5)	-6.5	5.1×10^{-10}	0.768	88 $4f^3(^4I^\circ)5f\ ^5M$	7 $4f^3(^4I^\circ)5f\ ^5L$	3 $4f^3(^2H2^\circ)5f\ ^3L$
e	$4f^3(^4I^\circ)5f\ ^5K$	5	114 021.3(4)	-18.0	5.1×10^{-10}	0.702	81 $4f^3(^4I^\circ)5f\ ^5K$	14 $4f^3(^4I^\circ)5f\ ^3I$	2 $4f^3(^2H2^\circ)5f\ ^3I$
⋮	⋮	⋮	⋮	⋮	⋮	⋮	⋮	⋮	⋮
e		8	130 935.4(*)		5.2×10^{-10}	1.020	51 $4f^3(^2H2^\circ)5f\ ^1L$	19 $4f^3(^2H2^\circ)5f\ ^3L$	10 $4f^3(^2H1^\circ)5f\ ^1L$
o	$4f^3(^4I^\circ)5d\ ^5L^\circ$	6	15 158.154(7)	-53.0	3.2×10^{-3}	0.724	93 $4f^3(^4I^\circ)5d\ ^5L^\circ$	3 $4f^3(^2H2^\circ)5d\ ^3K^\circ$	3 $4f^3(^4I^\circ)5d\ ^3K^\circ$
⋮	⋮	⋮	⋮	⋮	⋮	⋮	⋮	⋮	⋮
o		3	47 499.8(*)		1.5×10^{-6}	0.926	53 $4f^3(^4G^\circ)6s\ ^5G^\circ$	17 $4f^3(^2G1^\circ)6s\ ^3G^\circ$	13 $4f^3(^2G2^\circ)6s\ ^3G^\circ$
o	$4f^3(^4I^\circ)7s\ (^{\frac{9}{2}, \frac{1}{2}})^\circ$	4	103 085.765(10)	-5.7	1.4×10^{-9}	0.605	97 $4f^3(^4I^\circ)7s\ ^5I^\circ$	3 $4f^3(^2H2^\circ)7s\ ^3H^\circ$	
o	$4f^3(^4I^\circ)7s\ (^{\frac{9}{2}, \frac{1}{2}})^\circ$	5	103 335.469(8)	-2.7	1.4×10^{-9}	0.866	56 $4f^3(^4I^\circ)7s\ ^3I^\circ$	40 $4f^3(^4I^\circ)7s\ ^5I^\circ$	2 $4f^3(^2H2^\circ)7s\ ^3H^\circ$
o		1	103 359.1(*)		1.8×10^{-7}	1.000	59 $4f^3(^2F1^\circ)5d\ ^1P^\circ$	40 $4f^3(^2F2^\circ)5d\ ^1P^\circ$	
o	$4f^3(^4I^\circ)6d\ ^5K^\circ$	5	103 652.472(9)	2.6	1.1×10^{-9}	0.695	84 $4f^3(^4I^\circ)6d\ ^5K^\circ$	11 $4f^3(^4I^\circ)6d\ ^3I^\circ$	3 $4f^3(^2H2^\circ)6d\ ^3I^\circ$
⋮	⋮	⋮	⋮	⋮	⋮	⋮	⋮	⋮	⋮
o	$4f^3(^4I^\circ)6d\ ^3G^\circ$	5	111 138.018(18)	-26.2	1.3×10^{-9}	1.196	79 $4f^3(^4I^\circ)6d\ ^3G^\circ$	12 $4f^3(^4I^\circ)6d\ ^5G^\circ$	4 $4f^3(^4I^\circ)6d\ ^3H^\circ$

Notes. The full version of this table is available at the CDS with up to five leading eigenvector components for each energy level. The columns are: (1) parity, where ‘e’ is for even and ‘o’ is for odd, (2) assigned configuration and term label for levels experimentally found, (3) total angular momentum J , (4) experimentally determined or semi-empirically calculated level energy in this work, uncertainties are in parentheses in units of the final decimal place for experimental energies, an uncertainty ‘*’ indicates an experimentally unknown level, where only the calculated energy is shown, (5) difference between observed and calculated level energies, (6)–(8) lifetime due to electric dipole (E1) transitions, Landé g -factor, and three leading eigenvector percentages calculated using the Cowan code in this work.

uration. Lastly, the $4f^4 - 4f^37s$ and $4f^4 - 4f^35f$ interactions were scaled by 0.85 with respect to their corresponding Hartree-Fock values. The Cowan code calculations used for identifying levels of the present work were presented in Ding et al. (2024).

3.3.3. $4f^3(^4I^\circ)7s$ and $4f^3(^4I^\circ)6d$ levels

All 8 levels of the $4f^3(^4I^\circ)7s$ sub-configuration were identified and 38 of the 40 levels of the $4f^3(^4I^\circ)6d$ sub-configuration were identified. The $4f^36d - 4f^35f$ lines are around 8000 Å and calculated to have high TPs, but they lie outside the available sensitive spectral range of the Imperial College VUV FT spectrometer, so the known $4f^35f$ levels could not be used in the search for the unknown $4f^36d$ levels or vice versa.

As the $4f^36p$ configuration of Nd III is only well established for the $4f^3(^4I^\circ)$ parent term, only new $4f^3(^4I^\circ)7s$ and $4f^3(^4I^\circ)6d$ levels were identified in the present work, through classification of the newly observed $4f^36p - 4f^37s$ and $4f^36p - 4f^36d$ transitions. Attempts for these classifications were not successful using only the Nd-Ar PDL FT spectra and theoretical calculations from Gaigalas et al. (2019), where the $4f^37s$ and $4f^36d$ levels were predicted to have energies around 6000 cm^{-1} higher than their eventually observed values. Confident classifications of the transitions were first made in the Nd VS spectra, followed by confirmations with corresponding weak but more wavelength-accurate lines in the Nd-Ar PDL FT spectra. This initial progress improved the Cowan code parameter constraints and provided expectations for similar relative intensities in the FT and grating spectra for the other $4f^36p - 4f^37s$ and $4f^36p - 4f^36d$ transitions.

The two UV Nd-Ar PDL FT spectra contain only 3451 of the 21 584 lines fitted in total from all six spectra measured across the spectral range 11 500–54 000 cm^{-1} (8695–1852 Å) in Ding et al. (2024). The line densities across the spectral range are illustrated in Fig. 2. Compared to classifying the $4f^4 - 4f^35d$ transitions in the visible region, the lower line density and fewer number of blended lines above $\sim 30\,000\ \text{cm}^{-1}$ produced very few ambiguous classifications for the $4f^35d - 4f^36p$, $4f^36s - 4f^36p$, $4f^36p - 4f^37s$, and $4f^36p - 4f^36d$ transitions predicted (Gaigalas et al. 2019; Ding et al. 2024) to lie within this region. While the $4f^35d$ and $4f^36s - 4f^36p$ transitions were relatively straightforwardly classified in Ding et al. (2024), this was far more challenging for many $4f^36p - 4f^37s$ and $4f^36p - 4f^36d$ transitions; the strongest lines of these four transition arrays have similar predicted TPs, but the 7s and 6d levels lie about 40 000 cm^{-1} higher than the 6p levels. Therefore, due to lower level populations of the $4f^37s$ and $4f^36d$ levels, fewer $4f^36p - 4f^37s$ and $4f^36p - 4f^36d$ transitions were observed and were observed at lower S/Ns compared to the $4f^35d - 4f^36p$ and $4f^36s - 4f^36p$ transitions in the Nd-Ar PDL FT spectra. The reduction in line S/Ns and in the number of lines observed from each energy level increased the number of ambiguous classifications, hence many $4f^37s$ and $4f^36d$ levels could not be identified without the Nd VS grating spectra containing the weaker lines, especially in cases when only one line of a $4f^36d$ level was expected to be observable in the Nd-Ar PDL FT spectra.

In contrast, the number of lines measured in the Nd VS grating spectra between 1921–3250 Å was around 9000 and these were recorded under spectral resolving powers around one order

Table 2. Classified transitions of Nd III, originating from the $4f^2 7s$, $4f^2 6d$, and $4f^3 5f$ configurations, observed in the Nd-Ar PDL FT and Nd VS spectra (extract).

Spec	S/N	FWHM	Int.	$g_u A$	$\log(g_l/f)$	λ_{obs}	σ_{obs}	σ_{Ritz}	$\sigma_{\text{obs}} - \sigma_{\text{Ritz}}$	$\lambda_{\text{Ritz}}^{\text{air}}$	Lower Level	Upper Level	E_l	E_u	Note
(1)	(2)	(3)	(4)	(5)	(6)	(7)	(8)	(9)	(10)	(11)	Label	Label	(14)	(15)	(16)
g	1		1	3.1×10^9	-0.34	993.794(6)	100 624.4(6)	100 624.528(300)	-0.128	993.793(3)	$4f^3(4^1\text{D})5d^3\text{K}^{\circ}_7$	$4f^3(4^1\text{D})5f^3\text{I}_6$	18 656.272	119 280.8	
g	1		1	2.2×10^9	-0.49	994.019(6)	100 601.7(6)	100 601.732(300)	-0.032	994.019(3)	$4f^3(4^1\text{D})5d^3\text{K}^{\circ}_6$	$4f^3(4^1\text{D})5f^3\text{I}_5$	16 938.068	117 539.8	
g	0		0	1.8×10^9	-0.57	994.138(6)	100 589.7(6)	100 589.863(300)	-0.163	994.136(3)	$4f^3(4^1\text{D})5d^3\text{K}^{\circ}_5$	$4f^3(4^1\text{D})5f^3\text{I}_4$	15 262.437	115 852.3	
g	3		3	2.4×10^9	-0.45	997.327(6)	100 268.0(6)	100 268.628(300)	-0.628	997.321(3)	$4f^3(4^1\text{D})5d^3\text{K}^{\circ}_7$	$4f^3(4^1\text{D})5f^3\text{L}_8$	18 656.272	118 924.9	
g	5		5	4.8×10^9	-0.14	997.916(6)	100 208.8(6)	100 208.936(400)	-0.136	997.915(4)	$4f^3(4^1\text{D})5d^3\text{L}^{\circ}_8$	$4f^3(4^1\text{D})5f^3\text{M}_9$	18 861.064	119 070.0	
:	:	:	:	:	:	:	:	:	:	:	:	:	:	:	:
g	5		5	8.1×10^9	0.15	1083.318(6)	92 309.0(5)	92 309.079(400)	-0.079	1083.317(5)	$4f^3(4^1\text{D})5d^3\text{L}^{\circ}_9$	$4f^3(4^1\text{D})5f^3\text{L}_9$	28 877.321	121 186.4	
g	30		30	6.4×10^9	0.05	1084.030(6)	92 248.4(5)	92 248.215(300)	0.185	1084.032(4)	$4f^3(4^1\text{D})5d^3\text{L}^{\circ}_8$	$4f^3(4^1\text{D})5f^3\text{L}_8$	26 676.685	118 924.9	
g	40		40	2.2×10^{10}	0.59	1084.129(6)	92 239.9(5)	92 239.935(400)	-0.035	1084.129(5)	$4f^3(4^1\text{D})5d^3\text{L}^{\circ}_7$	$4f^3(4^1\text{D})5f^3\text{M}_8$	24 497.165	116 737.1	
g	2		2	3.9×10^9	-0.16	1085.156(6)	92 152.6(5)	92 152.735(300)	-0.135	1085.155(4)	$4f^3(4^1\text{D})5d^3\text{L}^{\circ}_7$	$4f^3(4^1\text{D})5f^3\text{L}_7$	24 497.165	116 649.9	
g	8		8	6.3×10^9	0.06	1107.003(6)	90 334.0(5)	90 334.035(300)	-0.035	1107.002(4)	$4f^3(4^1\text{D})5d^3\text{L}^{\circ}_7$	$4f^3(4^1\text{D})5f^3\text{M}_8$	24 497.165	114 831.2	
g	19		19	3.1×10^7	-1.66	2164.085(6)	46 208.92(13)	46 209.035(13)	-0.118	2163.3997(6)	$4f^3(4^1\text{D})6p^3\text{K}_6$	$4f^3(4^1\text{D})6d^3\text{K}^{\circ}_7$	62 520.646	108 729.681	
f	4		22	4.4×10^9	0.53	2254.5500(17)	44 354.749(33)	44 354.728(9)	0.021	2253.8528(5)	$4f^3(4^1\text{D})6p^3\text{I}_8$	$4f^3(4^1\text{D})6d^3\text{L}^{\circ}_9$	66 792.024	111 146.752	
f	6		24	3.3×10^9	0.40	2260.6456(9)	44 235.151(17)	44 235.150(10)	0.001	2259.9461(5)	$4f^3(4^1\text{D})6p^3\text{K}_7$	$4f^3(4^1\text{D})6d^3\text{L}^{\circ}_8$	64 622.006	108 857.156	
g	21		21	3.7×10^8	-0.55	2263.457(6)	44 180.21(12)	44 180.061(12)	0.150	2262.7643(6)	$4f^3(4^1\text{D})6p^3\text{I}_6$	$4f^3(4^1\text{D})6d^3\text{K}^{\circ}_7$	64 549.620	108 729.681	
g	49		49	7.1×10^8	-0.26	2264.787(6)	44 154.26(12)	44 154.232(14)	0.031	2264.0881(7)	$4f^3(4^1\text{D})6p^3\text{I}_4$	$4f^3(4^1\text{D})6d^3\text{G}^{\circ}_3$	60 638.963	104 793.195	
:	:	:	:	:	:	:	:	:	:	:	:	:	:	:	:
f	7		24	1.4×10^9	0.15	2599.5239(13)	38 468.583(19)	38 468.575(11)	0.008	2598.7476(7)	$4f^3(4^1\text{D})6p^3\text{K}_8$	$4f^3(4^1\text{D})7s(\frac{1}{2}, \frac{1}{2})^{\circ}_8$	70 599.570	109 068.145	
f	6		26	7.9×10^8	-0.10	2603.2166(16)	38 414.015(24)	38 414.008(11)	0.007	2602.4394(7)	$4f^3(4^1\text{D})6p^3\text{H}_7$	$4f^3(4^1\text{D})7s(\frac{1}{2}, \frac{1}{2})^{\circ}_6$	66 717.513	105 131.521	
f	18		62	2.2×10^9	0.35	2610.1592(5)	38 311.840(7)	38 311.836(6)	0.004	2609.3801(4)	$4f^3(4^1\text{D})6p^3\text{H}_6$	$4f^3(4^1\text{D})7s(\frac{3}{2}, \frac{1}{2})^{\circ}_5$	65 023.633	103 335.469	
f	2		6	6.9×10^7	-1.13	2679.0382(37)	37 326.829(52)	37 326.835(12)	-0.006	2678.2420(9)	$4f^3(4^1\text{D})6p^3\text{K}_8$	$4f^3(4^1\text{D})6d^3\text{K}^{\circ}_8$	70 599.570	107 926.405	
g	8		8	2.0×10^8	-0.66	2711.225(6)	36 883.69(8)	36 883.657(8)	0.035	2710.4244(6)	$4f^3(4^1\text{D})6p^3\text{K}_6$	$4f^3(4^1\text{D})7s(\frac{3}{2}, \frac{1}{2})^{\circ}_5$	66 451.812	103 335.469	

Notes. The full electronic version of this table is available at the CDS. The top half of this extract shows observed $4f^3 5d - 4f^3 5f$ transitions in the grating spectra, the bottom half shows $4f^3 6p - 4f^3 (7s + 6d)$ transitions observed in both the grating and FT spectra. The columns are: (1) spectrum of observation, where 'g' indicates line observed only in the grating Nd VS spectra and 'f' indicates line observed in both the Nd-Ar PDL FT and Nd VS spectra, where only the higher accuracy FT spectral lines are presented, (2)–(3) signal-to-noise ratio and full width at half maximum of the fitted FT spectral line, (4) approximate relative intensity corresponding to relative photon flux for 'f' and to relative energy flux for 'g', where lines above 2000 Å are on the same scale as those in Tables 6 and 7 of Ding et al. (2024) and lines below 2000 Å scale between 0 and 100. (5)–(6) weighted TP and log of the weighted (absorption) oscillator strength calculated using the Cowan code, where g_u and g_l refer to statistical weights of the upper and lower energy levels, respectively. (7)–(8) observed vacuum wavelength for 'g' and vacuum wavenumber for 'f', (9) Ritz wavenumber from level optimisation, (10) wavenumber difference between observed and Ritz values, (11) Ritz air wavelength for lines above 2000 Å converted using the three-term dispersion formula from Peck & Reeder (1972), Ritz vacuum wavelengths are given for lines below 2000 Å, (12)–(13) energy levels associated with the transition, their energies are in columns (14)–(15), respectively, and (16) contains comments of the observed transition, where 'B/W' indicates a blended or weak line with unreliable wavenumber and intensity, which was omitted from level optimisation. Uncertainties of columns (7), (8), and (9) are in parentheses in units of the final decimal place.

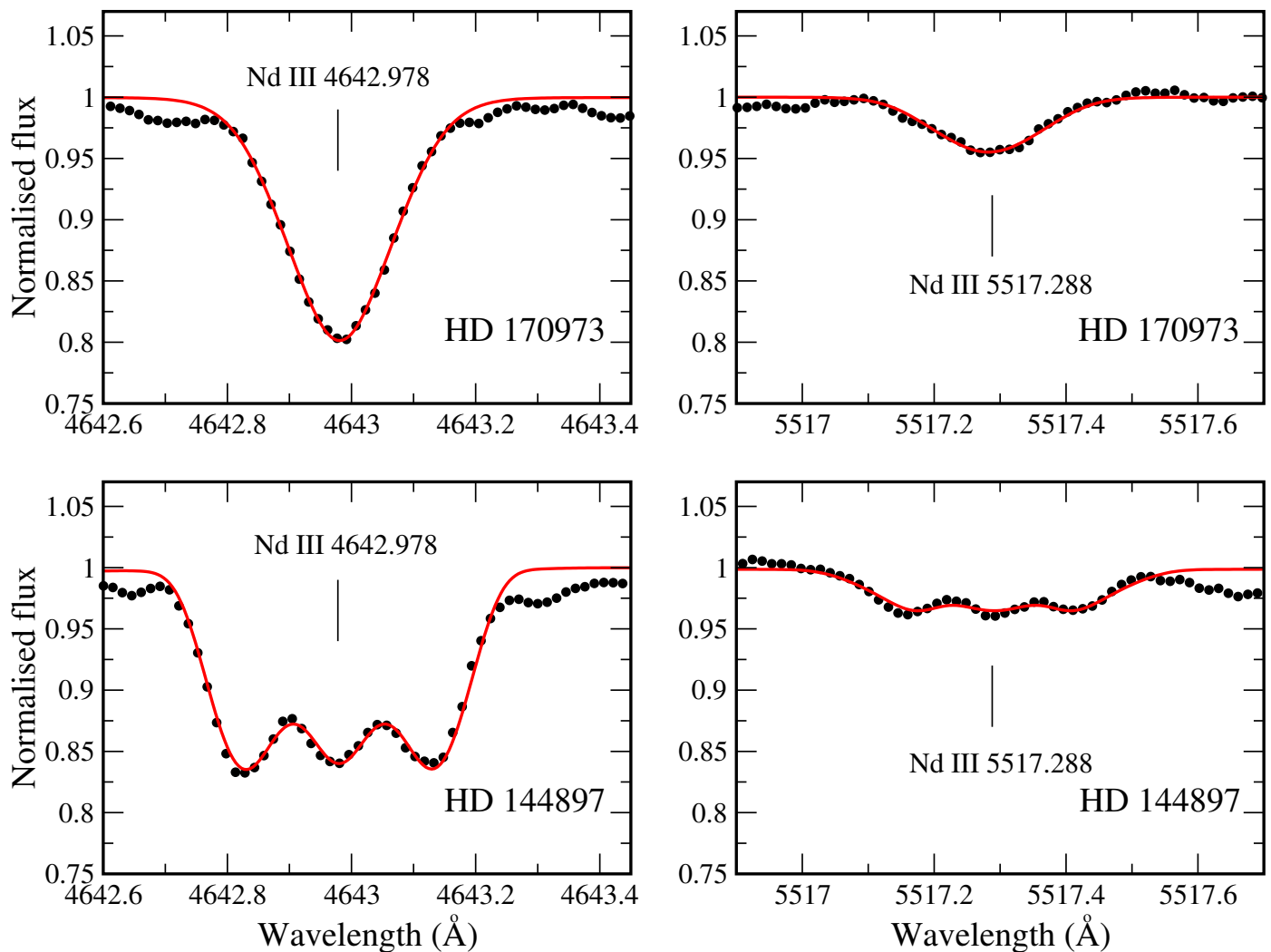


Fig. 1. Observed (black filled circles) and synthesised (red line) spectral lines of the newly identified $4f^3(^2H^{\circ})5d^3F^{\circ}_4$ level in spectra of HD 170973 and HD 144893 with surface magnetic fields $\langle B_s \rangle < 1$ kG and $\langle B_s \rangle = 8.8$ kG, respectively, showing two newly classified, previously unknown transitions of Nd III: $4f^4\ ^5F_5 - 4f^3(^2H^{\circ})5d^3F^{\circ}_4$ within 4642.6–4643.4 Å and $4f^4\ ^3H_4 - 4f^3(^2H^{\circ})5d^3F^{\circ}_4$ within 5516.9–5517.7 Å.

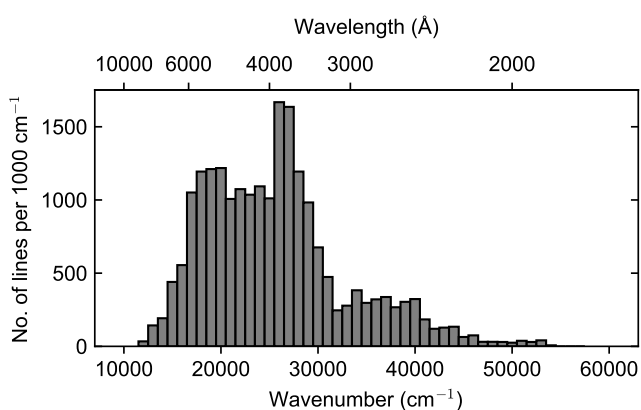


Fig. 2. The number of lines per 1000 cm^{-1} observed in the six Nd-Ar PDL FT spectra. We note that this distribution is largely dependent on the experimental parameters (see Table 2 of Ding et al. 2024), e.g., instrumental response and discharge conditions.

of magnitude lower than those in the Nd-Ar FT spectra, where

blended lines were expected to be very common at this line density. However, due to the much higher discharge currents, many $4f^36p - 4f^37s$ and $4f^36p - 4f^36d$ transitions were observed and their levels were confidently identified solely using the Nd VS grating spectra, which were later found to be consistent with the lines observed near the noise level in the Nd-Ar PDL FT spectra. Nevertheless, it was not possible to find the $4f^37s$ and $4f^36d$ levels with only a few transitions to known levels without corroboration with the Nd-Ar PDL FT spectra, e.g., many incorrect candidate lines were not observed or observed at unlikely relative intensities in the Nd-Ar PDL FT spectra.

3.3.4. $4f^35f$ levels

Based on the classification of 169 lines of the $4f^35d - 4f^35f$ transitions, 70 levels of the $5f$ configuration were found, containing all 56 levels of the $4f^3(^4I^{\circ})5f$ sub-configuration and 14 levels of the $4f^3(^4F^{\circ})5f$ and $4f^3(^2H^{\circ})5f$ sub-configurations. Transitions involving the $4f^35f$ levels were not observed in the Nd-Ar PDL FT spectra. As was mentioned previously, the wavelengths and intensities of the $4f^35d - 4f^35f$ transitions were taken from the line list of Wyart (2006) in the range 820–1159 Å. Only lines with intensities greater than 10 on this line list scale were defi-

Table 3. Configuration interaction space for the $4f^3(4f, 5f, 5d, 6d, \text{ and } 6p)$ (case 1) and $4f^3(7s + 6d)$ (case 2) singly excited configurations of Nd III.

Parity	Configurations
Even (both cases)	$(4f^4, 5p^5 4f^5), (4f^3 6p, 5p^5 4f^4 6p), 4f^2 5d^2, 4f^3 5f, 4f^2 5d 6s.$
Odd (case 1)	$(4f^3 5d, 5p^5 4f^4 5d), 4f^3 6d, (4f^3 6s, 5p^5 4f^4 6s), 4f^3 7s, 4f^2 5d 6p.$
Odd (case 2)	$4f^3 5d, (4f^3 6d, 5p^5 4f^4 6d), 4f^3 6s, (4f^3 7s, 5p^5 4f^4 7s), 4f^2 5d 6p.$

nity present in the Troitsk spectra. However, the intensity differences between the line lists of [Wyart \(2006\)](#) and Troitsk (of spectra recorded at two different spark currents) were used to aid classifications of lines belonging to Nd III.

4. New Nd III atomic structure and transition probability calculations

As the experimental energy level and spectrum analysis of Nd III concluded, final semi-empirical Cowan code calculations of Nd III fine structure and TPs were carried out. Results from these calculations are presented in this section.

4.1. Cowan Code parameters

The previous analysis of Nd III ([Ding et al. 2024](#)) did not include configurations involving the excitation of a $5p$ electron of the $5p^6$ core, where underestimations of the experimental lifetimes of five levels of Nd III ([Zhang et al. 2002](#)) were evident. Configuration interactions involving these $5p$ -excited configurations were shown to significantly increase calculated level lifetimes of Nd IV ([Wyart et al. 2007](#); [Arab et al. 2019](#)) and Nd V ([Meftah et al. 2008](#); [Deghiche et al. 2015](#)). To account for this in Nd III and to check the consistency of our energy level identifications, new semi-empirical calculations for Nd III were carried out using the Cowan code (e.g. [Cowan 1981](#); [Kramida 2021](#)) in the present work. The calculations presented here were made after the identification of all Nd III energy levels of this work.

Including all known configurations of Nd III and significant $5p$ -excited configurations of Nd III led to prohibitively large Hamiltonian matrix dimensions for our computational resources. Therefore, we included only the most significant configuration interactions of the $5p$ -excited configurations with the previously known and newly established energy levels, these are $5p^6 4f^4 \leftrightarrow 5p^5 4f^5$ and $5p^6 4f^3 6p \leftrightarrow 5p^5 4f^4 6p$ for the even parity, and $5p^6 4f^3 5d \leftrightarrow 5p^5 4f^4 5d$, $5p^6 4f^3 6s \leftrightarrow 5p^5 4f^4 6s$, $5p^6 4f^3 7s \leftrightarrow 5p^5 4f^4 7s$, and $5p^6 4f^3 6d \leftrightarrow 5p^5 4f^4 6d$ for the odd parity. Separate configuration interaction spaces were used in calculations for the $4f^3(4f, 5f, 5d, 6s, \text{ and } 6p)$ configurations (case 1) and $4f^3(7s + 6d)$ configurations (case 2). These two cases are presented in Table 3, where the aforementioned significant configuration interactions are indicated in parentheses.

Cowan code energy parameters for the $4f^3(7s, 6d, \text{ and } 5f)$ configurations are listed in Table 4. Configuration interaction parameters, and parameters of other configurations of Table 3 are available in the full version of Table 4 at the CDS. All Slater and configuration interaction parameters of the $5p$ -excited configurations were fixed at 0.85 and 0.7 of their ab initio HFR values, respectively. The calculated energy levels are presented in Table

Table 4. Parameters of the least-squares fit of energy levels of the $4f^3 7s$, $4f^3 6d$, and $4f^3 5f$ configurations of Nd III in the Cowan codes (extract).

Conf.	Param.	LSF ^a (cm ⁻¹)	G ^b	HFR ^a (cm ⁻¹)	Ratio ^{a,c}
4f ³ 7s	E_{av}	128 608(13)		120 146	8462
	$F^2(4f,4f)$	78 159(f)		102 509	0.762
	$F^4(4f,4f)$	53 201(f)		64 317	0.827
	$F^6(4f,4f)$	36 574(f)		46 270	0.790
	$\alpha(4f)$	22(f)		0	
	$\beta(4f)$	-600(f)		0	
	$\gamma(4f)$	1450(f)		0	
	$\zeta(4f)$	891(2)	1	956	0.932
	$G^3(4f,7s)$	714(76)		917	0.779
	4f ³ 6d	E_{av}	129 864(6)		121 138
$F^2(4f,4f)$		78 094(f)		102 424	0.762
$F^4(4f,4f)$		53 153(f)		64 259	0.827
$F^6(4f,4f)$		36 540(f)		46 227	0.790
$\alpha(4f)$		22(f)		0	
$\beta(4f)$		-600(f)		0	
$\gamma(4f)$		1450(f)		0	
$\zeta(4f)$		890(2)	1	955	0.932
$\zeta(6d)$		200(7)		174	1.146
$F^2(4f,6d)$		4389(183)		5283	0.831
$F^4(4f,6d)$		2251(338)		2328	0.967
$G^1(4f,6d)$		1372(56)		1938	0.708
$G^3(4f,6d)$		1782(203)		1723	1.034
$G^5(4f,6d)$	1172(115)		1355	0.864	
4f ³ 5f	E_{av}	139 658(21)		131 307	8351
	$F^2(4f,4f)$	76 479(124)		102 542	0.746
	$F^4(4f,4f)$	52 758(167)		64 340	0.820
	$F^6(4f,4f)$	36 567(f)		46 287	0.790
	$\alpha(4f)$	22(f)		0	
	$\beta(4f)$	-600(f)		0	
	$\gamma(4f)$	1450(f)		0	
	$\zeta(4f)$	885(2)		956	0.926
	$\zeta(5f)$	21(7)		21	1.000
	$F^2(4f,5f)$	2579(131)		4027	0.641
	$F^4(4f,5f)$	1404(282)		1575	0.891
	$F^6(4f,5f)$	877(148)		1010	0.868
	$G^0(4f,5f)$	879(16)		2811	0.313
	$G^2(4f,5f)$	990(118)		1846	0.536
	$G^4(4f,5f)$	976(241)		1238	0.788
$G^6(4f,5f)$	788(105)		911	0.864	

Notes. The full version of this table is available at the CDS, including parameters corresponding to the interaction space of Table 4. ^(a) Parameter values determined in the ab initio pseudo-relativistic Hartree–Fock (HFR) and least-squares-fitted (LSF) calculations and their ratio. Standard deviations of the fitted LSF parameters are in parentheses, where ‘f’ means the parameter was fixed. ^(b) Parameters in each numbered group (G) were linked together by sharing the same ratios to their corresponding HFR values. ^(c) Differences between LSF and HFR parameters are given for E_{av} in this extract.

1, but levels predicted in the odd system with energies between 47 500 and 103 085 cm⁻¹ are not included, because they are ex-

pected to be very uncertain due to the lack of known levels in this energy range in the odd parity.

4.2. Transition probabilities and energy level lifetimes

The calculated TPs are presented in Table 5. The wavelength range (1900–50 000 Å) is selected for the applicability of the data in vacuum-UV–mid-IR spectroscopic studies. Based on line strength significance and accuracy, the range of transitions presented is as follows: 1900–50 000 Å and $g_u A > 10^3 \text{ s}^{-1}$ for transitions of the $4f^3(4f, 5d, 6s, \text{ and } 6p)$ configurations with even parity level energies below 131 000 cm^{-1} and odd parity below 47 500 cm^{-1} (calculated under case 1 of Table 3), 2060–2950 Å and $g_u A > 10^3 \text{ s}^{-1}$ for transitions with upper levels from the $4f^3(7s + 6d)$ configurations with even parity level energies below 80 700 cm^{-1} and odd parity level energies within 103 000–112 000 cm^{-1} (calculated under case 2 of Table 3), and 3700–30 000 Å and $g_u A > 10^4 \text{ s}^{-1}$ for transitions with lower levels from the $4f^3(7s + 6d)$ configurations with even parity level energies below 131 000 cm^{-1} and odd parity level energies within 103 000–112 000 cm^{-1} (calculated under case 2 of Table 3).

The uncertainties in the calculated TPs and branching ratios are indicative from the cancellation factors (Cowan 1981) in Table 5. Smaller cancellation factors indicate larger uncertainties due to larger destructive interference in the summations of the dipole matrix element evaluation. For context, around 90% of the transitions of Nd III observed in the laboratory are calculated to have cancellation factors greater than 0.05. The calculated branching ratios of these lines were compared with their experimental relative intensities in their classifications (Ding et al. 2024).

Level lifetimes of the $4f^3 5d$ configuration calculated in the present work from additionally considering 5p-excited configurations are on average 60% larger compared to those calculated in Ding et al. (2024). This improved the mean ratio between the five experimental lifetimes measured by Zhang et al. (2002) and their calculated values from 1.4 to 0.9. However, the root-mean-square deviation from the five experimental values increased from 61 to 88 ns. Furthermore, the changes in lifetime for levels of other configurations (not $4f^3 5d$) were less than 10% when 5p-excited configuration interactions of the present work are included, indicated by transitions with $g_u A > 10^7 \text{ s}^{-1}$. To reduce computational complexity, the $5p^6 4f^3 5f \leftrightarrow 5p^5 4f^4 5f$ configuration interaction was not included due to negligible changes observed for the $4f^3 5f$ lifetimes when included. We expect more lifetime measurements for Nd III levels to be required to conclude whether the present lifetime calculations provide improvements compared to those made in Ding et al. (2024).

We would also like to note that the lifetimes calculated in the present work in Table 1 are only from electric dipole (E1) transitions, so lifetimes are not listed for levels with no lower level of opposite parity or J value within ± 1 , e.g., the lowest-lying $4f^4$ levels labelled with 5I , 5F , and 3K2 terms.

4.3. Implications for the Nd III energy level analysis

The implications of the new calculations including 5p-excited configuration interactions on all experimental identification of Nd III energy levels were investigated. The lowest levels of the 5p-excited configurations were estimated to lie several 10 000 cm^{-1} above the highest-lying known level. Therefore, changes to eigenvector compositions and branching fractions of known levels were very small. None of the five leading eigenvec-

tor components of the levels of Table 1 belong to the 5p-excited configurations. Experimental energy level identifications using calculations without 5p-excited configuration interactions (Table 1 and Ding et al. 2024) agree with calculations from the present work including 5p-excited configuration interactions. In a few cases, branching fractions obtained in the new calculations with 5p-excited configuration interactions agreed better with experimental relative intensities. Only two of the highest-lying $4f^3 6p$ levels reported in Ding et al. (2024), 77 231.115 cm^{-1} $J = 5$ and 80 593.604 cm^{-1} $J = 6$, are now considered uncertain and tentative due to results of the new calculations. This does not affect the optimised energies of other levels as the energies of these two levels are defined by one line each.

4.4. Evaluation using Nd-rich stellar spectra

Nd III TPs calculated in the present work offer improvements to those from Gaigalas et al. (2019) and Ding et al. (2024). We deduced this by comparing Nd abundance determined using $4f^4 - 4f^3 5d$ transitions in the Nd-rich star HD 170973 with values obtained using experimental Nd II TPs (Den Hartog et al. 2003). The comparison is shown in Fig. 3. The analysed Nd II and Nd III spectral lines are listed in Table 6 and Table 7, respectively, where $\log \epsilon_{\text{Nd}} = \log(N_{\text{Nd}}/N_{\text{tot}}) + 12.04$ for number densities of neodymium N_{Nd} and of the total number of atoms N_{tot} . Abundances were derived by fitting synthetic Nd II-III line profiles to observed features using a model atmosphere with effective temperature $T_{\text{eff}} = 11200 \text{ K}$ and surface gravity $\log g = 3.8$ (Ryabchikova et al. 2011). According to the analysis of rare-earth abundances in Ap star atmospheres as a function of effective temperature (Ryabchikova & Romanovskaya 2017, see Fig. 2 of their paper), Nd ionisation equilibrium is observed in the temperature range 10 000 – 12 000 K. Therefore we may expect Nd abundance from Nd II and Nd III lines to agree for HD 170973, which we have observed with the present TP calculations of this work. We note that $\log \epsilon_{\text{Nd}}$ obtained using TPs of Ding et al. (2024), calculated without considering 5p-excitation (not shown), are about 0.2 dex lower, indicating the improvements of the present calculations.

The difficulty in using the Nd III TP data calculated by Gaigalas et al. (2019) for the interpretation of the stellar spectra should be mentioned. Many calculated levels in the Gaigalas et al. (2019) dataset have been labelled with the same names. For example, in the $J = 6$ matrix, the 20777.62 and 21844.68 cm^{-1} levels have (in their notations) the $4f(3)4I1.5d_5I$ label, the 25161.85 and 26820.84 cm^{-1} levels have the $4f(3)4I1.5d_5G$ label, the 32640.91 and 32961.13 cm^{-1} levels are attributed to the $4f(3)4F1.5d_5H$ label, and so on. We can illustrate impacts of such ambiguity in the interpretation of the HD 170973 stellar spectrum using an example of the experimentally known transition $4f^4 \ ^3K2_6 - 4f^3 5d(^4F^o)5d \ ^5H^o_6$ at 5852.43 Å. As is expected, the calculated $\log(gf)$ values are different for the transitions from the two levels of the same label as given in Gaigalas et al. (2019). The differences in spectral syntheses between these two $\log(gf)$ s are shown by blue and dashed blue lines in Fig. 4. The $\log(gf)$ used for the blue line appears to be the correct value, agreeing with the average abundance deviation. However, the $\log(gf)$ used for the dashed blue line belongs to the predicted level that better resembled the known $4f^3 5d(^4F^o)5d \ ^5H^o_6$ level at 31146.457 cm^{-1} , based on relative intensity analysis of the stronger observed and predicted lines to the ground term levels and from $4f^3(^4F^o)6p \ ^5G_5$. All other Nd III transitions from Gaigalas et al. (2019) used in the abundance determinations

Table 5. Calculated TPs using configuration interaction spaces of Table 3 (extract).

Type	CF	$g_u A$ (s^{-1})	$\log(g_{lf})$	σ_{Ritz} (cm^{-1})	λ_{Ritz} (\AA)	$\lambda_{\text{Ritz}}^{\text{air}}$ (\AA)	Lower Level Term Label	J_l	Upper Level Term Label	J_u	E_l (cm^{-1})	E_u (cm^{-1})	g_l^l	g_u^l
(1)	(2)	(3)	(4)	(5)	(6)	(7)	(8)	(9)	(10)	(11)	(12)	(13)	(14)	(15)
2	0.01	2.2×10^6	-2.92	52 659.745(*)	1898.9837(*)	1898.3517	$4f^2(^1D^{\circ})5d^5F^{\circ}$	4	$4f^2(^3H)5d(^2D)(^4G)6s^5G$	3	47 404.355	100 064.1	1.223	0.944
2	0.00	6.0×10^5	-3.49	52 648.771(*)	1899.3796(*)	1898.7474	$4f^3(^4F)6s(\frac{1}{2}, \frac{1}{2})^{\circ}$	5	$4f^2(^3F)5d(^3F)^5G$	5	32 309.729	84 958.5	0.875	1.201
2	0.00	2.9×10^6	-2.80	52 645.550(*)	1899.4958(*)	1898.8636	$4f^3(^2H)5d^1G^{\circ}$	4	$4f^2(^3H)5d(^3P)^5H$	5	36 517.350	89 162.9	1.067	1.173
2	0.08	8.0×10^7	-1.36	52 643.587(*)	1899.5666(*)	1898.9344	$4f^3(^4F^{\circ})5d^3H^{\circ}$	4	$4f^3(^2D)6p^3F$	3	32 077.113	84 720.7	0.948	1.076
2	0.01	4.4×10^6	-2.62	52 636.914(*)	1899.8074(*)	1899.1752	$4f^3(^2H)5d^2K^{\circ}$	6	$4f^2(^3H)5d(^3F)^5H$	7	29 643.186	82 280.1	0.990	1.133
:	:	:	:	:	:	:	:	:	:	:	:	:	:	:
2	0.12	1.1×10^6	-2.44	21 331.734(*)	4687.8514(*)	4686.5398	$4f^3(^4F^{\circ})6d^3H^{\circ}$	5	$4f^3(^4F^{\circ})5f^3G$	5	108 852.966	130 184.7	1.087	1.165
1	0.00	2.3×10^3	-5.12	21 328.712(*)	4688.5156(*)	4687.2038	$4f^3(^2H)6s^3H^{\circ}$	5	$4f^3(^4F^{\circ})6p^3I$	5	43 022.1	64 350.812	1.129	0.849
R	0.01	2.2×10^5	-3.14	21 325.613(800)	4689.1970(1800)	4687.8850	$4f^3(^4F^{\circ})6d^3I^{\circ}$	6	$4f^3(^4F^{\circ})5f^5I$	6	105 866.787	127 192.4	0.966	1.052
L	0.11	4.5×10^6	-1.83	21 320.284(6)	4690.3690(13)	4689.0567	$4f^4^5I$	7	$4f^2(^4F^{\circ})5d^3H^{\circ}$	6	37 14.548	25 034.832	1.177	1.241
2	0.01	1.1×10^4	-4.44	21 319.013(*)	4690.6487(*)	4689.3363	$4f^3(^4F^{\circ})6d^5H^{\circ}$	4	$4f^2(^1D)5d(^2D)(^2H)6s^3H$	5	106 265.687	127 584.7	0.993	1.108
:	:	:	:	:	:	:	:	:	:	:	:	:	:	:
12	0.10	8.6×10^3	-2.55	21 26.8(*)	47 019.00(*)	47 006.18	$4f^3(^2K^{\circ})5d^1H^{\circ}$	5	$4f^4^1G3$	4	46 408.0	48 534.8	1.014	1.005
1	0.03	1.4×10^3	-3.32	2089.525(*)	47 857.7667(*)	47 844.7207	$4f^4^3F2$	3	$4f^3(^4F^{\circ})5d^3G^{\circ}$	4	24 050.7	26 140.225	1.113	1.060
1	0.05	1.3×10^3	-3.34	2059.925(*)	48 545.4568(*)	48 532.2233	$4f^4^3M$	8	$4f^3(^4F^{\circ})5d^3I^{\circ}$	7	21 943.3	24 003.225	0.948	1.171
1	0.07	1.6×10^3	-3.23	2007.711(*)	49 807.9654(*)	49 794.3880	$4f^4^3I1$	7	$4f^3(^4F^{\circ})5d^3K^{\circ}$	8	25 434.2	27 441.911	1.137	1.138
12	0.02	1.8×10^3	-3.17	2005.9(*)	49 852.93(*)	49 839.34	$4f^4^3H3$	5	$4f^3(^2G1^{\circ})5d^3H^{\circ}$	5	38 143.2	40 149.1	1.028	1.120

Notes. The electronic version of this table is available at the CDS. In Col. 1, the label '1' indicates (experimentally) unknown lower level, '2' indicates unknown upper level, '12' indicates that both levels are unknown, 'L' indicates a transition observed in the laboratory, and 'R' indicates a transition with known levels but unobserved in the laboratory. The remaining columns are: (2) cancellation factor as defined in (Cowan 1981), (3)–(4) weighted TP, and log of the weighted (absorption) oscillator strength, where g_u and g_l refer to statistical weights of the upper and lower energy levels, respectively, (5)–(7) vacuum Ritz wavenumber, vacuum Ritz wavelength, and air Ritz wavelength converted using the three term dispersion formula from (Peck & Reeder 1972), respectively, where uncertainties are given in parentheses in units of the final decimal places for lines with types 'L' and 'R', otherwise, '*' indicates at least one unknown energy level for a transition, (8)–(13) level term labels, J values, and energies, where the term labels of unknown levels are from the leading eigenvectors in the LS coupling scheme, and (14)–(15) upper and lower level Landé g -factors.

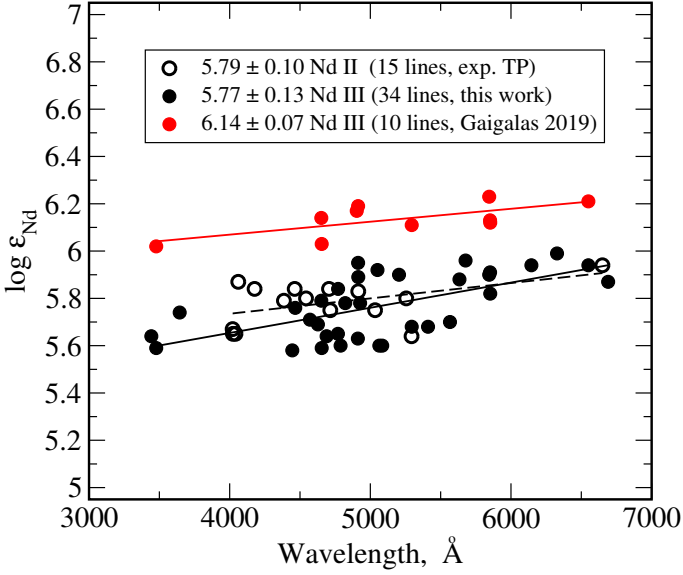


Fig. 3. Nd abundance $\log \varepsilon_{\text{Nd}}$ in the star HD 170973 against wavelength determined using experimental Nd II TPs (open black, Den Hartog et al. 2003) and Nd III TPs of this work (filled black circles) and of Gaigalas et al. (2019) (filled red circles). Mean values and their uncertainties are in the legend. Linear regressions are shown by solid and dashed lines.

Table 6. Nd II spectral lines used for Nd abundance determination of HD 170973.

λ^{air} (Å)	E_l (eV)	$\log(g_l f)$	$\log \varepsilon_{\text{Nd}}$
4021.327	0.321	-0.10	5.67
4023.000	0.559	0.04	5.65
4041.056	0.471	-0.53	5.65
4061.080	0.471	0.55	5.87
4177.320	0.064	-0.10	5.84
4385.661	0.205	-0.30	5.79
4462.409	0.205	-0.91	5.84
4542.600	0.742	-0.28	5.80
4706.543	0.000	-0.71	5.84
4715.586	0.205	-0.90	5.75
4914.382	0.380	-0.70	5.83
5033.507	1.136	-0.47	5.75
5255.506	0.205	-0.67	5.84
5293.163	0.823	0.10	5.64
6650.517	1.953	-0.11	5.94

Notes. Using air wavelength λ^{air} , lower level energy E_l , and $\log(g_l f)$ from Den Hartog et al. (2003).

of HD 170973 shown in Fig. 3 were to the ground term levels. These transitions are expected to not have ambiguous labels and hence comparable with our results. Therefore, we highlight the advantages of the present work in individual line position and stellar spectra analyses. Although in the context of kilonova opacity calculations, the difference between TPs of the present work and those from Gaigalas et al. (2019) may not be significant, we do however expect the newly established Ritz wave-

Table 7. Nd III spectral lines used for Nd abundance determination of HD 170973.

λ^{air} (Å)	E_l (eV)	$\log(g_l f)$ (This work)	$\log \varepsilon_{\text{Nd}}$ (This work)	$\log(g_l f)$ (Gaigalas et al. 2019)	$\log \varepsilon_{\text{Nd}}$ (Gaigalas et al. 2019)
3442.7834	0.141	-1.73	5.64		
3477.8330	0.000	-1.85	5.59	-2.31	6.02
3644.3510	0.461	-0.78	5.74		
4445.0012	0.296	-2.33	5.58		
4466.3512	0.461	-2.54	5.76		
4570.6374	0.141	-2.14	5.71		
4627.2556	0.461	-2.38	5.69		
4651.6172	0.000	-2.07	5.79	-2.39	6.11
4654.3195	0.000	-1.94	5.59	-2.45	6.03
4689.0565	0.461	-1.83	5.64		
4769.6184	0.296	-1.86	5.65		
4770.8900	1.510	-1.72	5.84		
4788.4584	0.461	-1.92	5.60		
4821.9906	0.296	-2.78	5.78		
4903.2380	0.000	-2.53	5.89	-3.36	6.17
4911.6527	0.141	-1.74	5.63		
4912.9436	0.000	-1.94	5.95	-2.32	6.19
4914.0941	0.461	-1.27	5.89		
4927.4877	0.461	-1.00	5.78		
5050.6952	0.296	-1.24	5.92		
5084.6597	0.141	-2.65	5.60		
5203.9236	0.141	-0.83	5.90		
5294.1133	0.000	-0.85	5.68	-1.19	6.11
5410.0994	0.141	-1.62	5.68		
5566.0154	0.296	-2.46	5.70		
5633.5540	0.141	-2.29	5.88		
5677.1788	0.631	-1.62	5.96		
5845.0201	0.631	-1.32	5.90	-1.61	6.23
5851.5419	0.461	-1.69	5.91	-1.91	6.13
5852.4312	1.744	-1.60	5.82	-1.90	6.12
6145.0677	0.296	-1.48	5.94		
6327.2649	0.141	-1.55	5.99		
6550.2242	0.000	-1.64	5.94	-1.97	6.21
6690.8302	0.461	-2.57	5.87		

lengths to allow improvements in any kilonovae spectral feature determinations.

5. Revision of Nd III ionisation energy

The ionisation energy of Nd III is the energy separation between the $4f^4 \ ^5I_4$ ground energy level of Nd III and the $4f^3 \ ^4I_{9/2}$ ground energy level of Nd IV, which can be estimated when the four levels of the $4f^3(^4I_{9/2})6s$ and $4f^3(^4I_{9/2})7s$ sub-configurations of Nd III are known (Sugar & Reader 1973). The method is based on solving the equation of the difference between the center-of-gravity (COG) binding energies of the $4f^3 6s$ and $4f^3 7s$ configu-

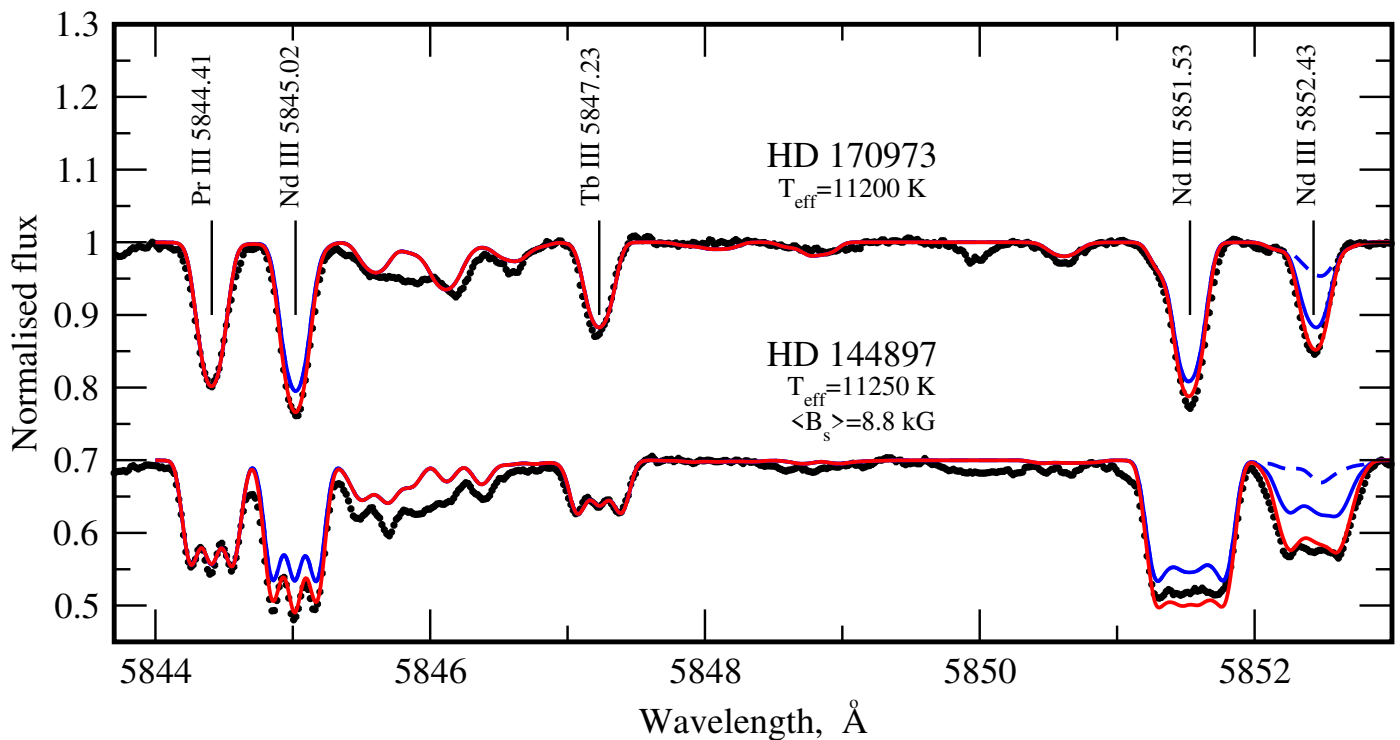


Fig. 4. Observed (black filled circles) spectra in the interval 5844–5853 Å of stars HD 170973 and HD 144893 with surface magnetic fields $\langle B_s \rangle < 1$ kG and $\langle B_s \rangle = 8.8$ kG, respectively, the coloured lines show fits to the observed spectra using Nd abundances $\log \epsilon_{\text{Nd}} = 5.84$ and 5.77, respectively. Fits using TPs calculated in the present work are in red and fits using TPs from Gaigalas et al. (2019) are in blue and dashed blue. All Landé g -factors used are calculated from the present work.

rations using the Rydberg-Ritz formula,

$$\Delta T = \frac{R_{\text{Nd}} Z_C}{[n^*(6s)]^2} - \frac{R_{\text{Nd}} Z_C}{[n^*(6s) + \Delta n^*(7s - 6s)]^2}, \quad (1)$$

where $R_{\text{Nd}} = 109\,736.9$ cm $^{-1}$ is the Nd Rydberg constant, $Z_C = 3$ is the Nd III core charge, $n^*(ns)$ is the effective quantum number of the configuration ns , and $\Delta n^*(7s - 6s) = n^*(7s) - n^*(6s)$. The ΔT of Nd III, defined for the full 6s and 7s configurations, is well represented by the difference between COG energies the lowest-lying terms of the $4f^3(4I_{9/2}^\circ)6s$ and $4f^3(4I_{9/2}^\circ)7s$ sub-configurations (Sugar & Reader 1965; Reader & Sugar 1966; Sugar & Reader 1973). Thus, with knowledge of the quantities ΔT and $\Delta n^*(7s - 6s)$, $n^*(6s)$ and hence the COG binding energy of $4f^3(4I_{9/2}^\circ)6s$ is solved, which is added to the COG energy of $4f^3(4I_{9/2}^\circ)6s$ relative to the ground state energy to yield the ionisation energy.

In 1973, the COG energies of the $4f^3(4I_{9/2}^\circ)6s$ and $4f^3(4I_{9/2}^\circ)7s$ sub-configurations were unknown. These quantities, as well as $\Delta n^*(7s - 6s)$, were interpolated by Sugar & Reader (1973) from studies of some second and third spectra of the lanthanide atoms. With the accepted quantity $\Delta n^*(7s - 6s) = 1.048 \pm 0.002$, the ionisation energy was estimated in 1973 as $178\,600 \pm 2400$ cm $^{-1}$.

Recently, Johnson & Nelson (2017b) updated the Nd III ionisation energy to be $178\,140 \pm 600$ cm $^{-1}$ using a framework of the method by Sugar & Reader (1973). The levels of the $4f^3(4I_{9/2}^\circ)6s$ and $4f^3(4I_{9/2}^\circ)7s$ sub-configurations were still unknown. However, improved interpolated values of ΔT and $\Delta n^*(7s - 6s)$ were obtained from the availability of new data since 1973 for the other neighbouring ions.

In Ding et al. (2024) and the present work, the COG energies of the $4f^3(4I_{9/2}^\circ)6s$ and $4f^3(4I_{9/2}^\circ)7s$ sub-configurations

were determined at $30\,269$ cm $^{-1}$ and $103\,223$ cm $^{-1}$ respectively, this corresponds to $\Delta T = 72\,954$ cm $^{-1}$ and has now permitted a further update of the Nd III ionisation energy. Together with the estimated value of $\Delta n^*(7s - 6s) = 1.0476 \pm 0.0052$ by Johnson & Nelson (2017b), 2.5850 is now obtained for $n^*(6s)$. As a result, the ionisation energy of Nd III is estimated to be $178\,070 \pm 330$ cm $^{-1}$, in close agreement with Johnson & Nelson (2017b) but with about two times higher accuracy. The uncertainty ± 330 cm $^{-1}$ is at two standard deviations and is fully determined by the ± 0.0052 uncertainty of the $\Delta n^*(7s - 6s)$ value estimated by Johnson & Nelson (2017a).

6. Outlook

This work has made significant progress with new levels of the singly excited configurations of Nd III. Energy levels of the doubly-excited configurations of Nd III (e.g. $4f^25d^2$, $4f^25d6s$, and $4f^25d6p$), however, remain experimentally unknown. Experimentally determining their level energies should further improve atomic structure and TP calculations of Nd III as these overlap greatly with the configurations of known levels. More than half of the lines measured (observed) in the FT and grating spectra remain unclassified, this number is of order 10^4 . Therefore, the accurate experimental knowledge of the spectra of Nd in its first few ionisation stages is still appreciably incomplete. Further analyses of these spectra are expected to be more challenging compared to the presented work and the work of Ding et al. (2024), and more extensive experimental measurements are also likely required.

7. Summary

Fourier transform spectroscopy of Nd-Ar Penning and hollow cathode discharge lamps, grating spectroscopy of Nd vacuum sliding sparks, and the parameterised Cowan code atomic structure and TP calculations have enabled the first experimental classification of 355 transitions and establishment of 116 new energy levels of the $4f^3 7s$, $4f^3 6d$, and $4f^3 5f$ configurations of Nd III. One previously unknown level of the $4f^3 5d$ configuration is also now identified. Together with results from Ding et al. (2024), 261 energy levels and 972 transitions of Nd III have been observed, classified, and measured at accuracies up to a few parts in 10^8 . The experimentally determined energies of the four levels of the $4f^3(4I_{9/2})6s$ and $4f^3(4I_{9/2})7s$ sub-configurations enabled a revision of the Nd III ionisation energy at $178\,070 \pm 330 \text{ cm}^{-1}$. Calculated level energies, eigenvector compositions, and lifetimes are presented for energies within $15\,158\text{--}47\,500 \text{ cm}^{-1}$ and $103\,085\text{--}111\,165 \text{ cm}^{-1}$ for the odd parity system and within $0\text{--}130\,936 \text{ cm}^{-1}$ for the even parity system. Transition wavelengths with significant calculated TPs within $1900\text{--}50\,000 \text{ \AA}$ are also presented and evaluated against stellar spectra. These new data will aid future experimental and theoretical investigations of the Nd III spectrum and allow more accurate and reliable modeling of astrophysical plasmas containing Nd III, such as in stellar atmospheres and kilonovae.

Acknowledgements. This work was supported at Imperial College by the STFC of the UK, grant numbers ST/S000372/1, ST/N000838/1, and ST/W000989/1, the Bequest of Prof. Edward Steers, and at the Institute of Spectroscopy of the Russian Academy of Sciences the research project FFUU-2022-0005. We are grateful to Prof. C. R. Cowley for sharing the unpublished Nd III line lists of Dr H. M. Crosswhite. We also thank Dr J.-F. Wyart and Prof. W.-Ü. Tchang-Brillet for providing the Nd vacuum sliding spark grating plates recorded at NIST, and we acknowledge Dr N. Spector and Dr J. Sugar for the recording of these plates.

References

- Aldenius, M. 2001, Master's thesis, University of Lund
 Arab, K., Deghiche, D., Meftah, A., et al. 2019, JQSRT, 229, 145
 Cowan, J. J., Sneden, C., Lawler, J. E., et al. 2021, RMP, 93, 015002
 Cowan, R. D. 1981, The theory of atomic structure and spectra (Univ of California Press)
 Cowley, C. R., Ryabchikova, T., Kupka, F., et al. 2000, MNRAS, 317, 299
 Deghiche, D., Meftah, A., Wyart, J.-F., et al. 2015, Physica Scripta, 90, 095402
 Den Hartog, E., Lawler, J., Sneden, C., & Cowan, J. 2003, ApJS, 148, 543
 Dieke, G. & Crosswhite, H. 1963, Appl. Opt., 2, 675
 Dieke, G., Crosswhite, H., & Dunn, B. 1961, JOSA, 51, 820
 Ding, M. 2024, PhD thesis, Imperial College London
 Ding, M., Ryabtsev, A. N., Kononov, E. Y., et al. 2024, A&A, 684, A149
 Domoto, N., Tanaka, M., Kato, D., et al. 2022, ApJ, 939, 8
 Even, W., Korobkin, O., Fryer, C. L., et al. 2020, ApJ, 899, 24
 Finley, D. S., Bowyer, S., Paresce, F., & Malina, R. F. 1979, Appl. Opt., 18, 649
 Gaigalas, G., Kato, D., Rynkun, P., Radžiūtė, L., & Tanaka, M. 2019, ApJS, 240, 29
 Heise, C., Hollandt, J., Kling, R., Kock, M., & Kühne, M. 1994, Appl. Opt., 33, 5111
 Johnson, D. A. & Nelson, P. G. 2017a, JPCRD, 46, 013108
 Johnson, D. A. & Nelson, P. G. 2017b, JPCRD, 46, 013109
 Kasen, D., Badnell, N., & Barnes, J. 2013, ApJ, 774, 25
 Kramida, A. 2011, CoPhC, 182, 419
 Kramida, A. 2021, A suite of atomic structure codes originally developed by RD Cowan adapted for Windows-based personal computers, National Institute of Standards and Technology: Gaithersburg, MD, USA
 Kramida, A., Ralchenko, Y., Reader, J., & the NIST ASD Team. 2022, NIST Atomic Spectra Database (version 5.10), National Institute of Standards and Technology, Gaithersburg, MD
 Learner, R. & Thorne, A. 1988, JOSAB, 5, 2045
 Meftah, A., Wyart, J.-F., Sinzelle, J., et al. 2008, Physica Scripta, 77, 055302
 Peck, E. R. & Reeder, K. 1972, JOSA, 62, 958
 Przybylski, A. 1977, MNRAS, 178, 71
 Reader, J. & Sugar, J. 1966, JOSA, 56, 1189
 Ryabchikova, T., LeBlanc, F., & Shulyak, D. 2011, in Magnetic Stars, 69–80

- Ryabchikova, T., Ryabtsev, A., Kochukhov, O., & Bagnulo, S. 2006, A&A, 456, 329
 Ryabchikova, T. A. & Romanovskaya, A. M. 2017, Astronomy Letters, 43, 252
 Savanov, I., Malanushenko, V., & Ryabchikova, T. 1999, Astronomy Letters, 25, 802
 Smartt, S., Chen, T.-W., Jerkstrand, A., et al. 2017, Nature, 551, 75
 Sugar, J. & Reader, J. 1965, JOSA, 55, 1286
 Sugar, J. & Reader, J. 1973, JChPh, 59, 2083
 Tanaka, M. & Hotokezaka, K. 2013, ApJ, 775, 113
 Tanaka, M., Kato, D., Gaigalas, G., & Kawaguchi, K. 2020, MNRAS, 496, 1369
 Tanaka, M., Kato, D., Gaigalas, G., et al. 2018, ApJ, 852, 109
 Thorne, A., Harris, C., Wynne-Jones, I., Learner, R., & Cox, G. 1987, JPhE, 20, 54
 Watson, D., Hansen, C. J., Selsing, J., et al. 2019, Nature, 574, 497
 Whaling, W., Anderson, W., Carle, M., Brault, J., & Zarem, H. 1995, J. Quant. Spectr. Rad. Transf., 53, 1
 Wyart, J.-F. 2006, private communication
 Wyart, J.-F., Meftah, A., Tchang-Brillet, W.-Ü. L., et al. 2007, JPhB, 40, 3957
 Zhang, Z., Svanberg, S., Palmeri, P., Quinet, P., & Biémont, E. 2002, A&A, 385, 724